EFP Analyzer: A fast, accurate, and easy-to-teach program for analyzing Extracellular Field Potentials from iPSC-derived cardiomyocytes

Nidhi Patel[1#], Alex Shen[1#], Yuko Wada[1], Marcia Blair[1], Devyn Mitchell[1], Loren Vanags[1], Suah Woo[1], Matthew Ku[1], Kundivy Dauda[1], William Morris[1], Minjoo Yang[1], Björn C. Knollmann[1,2], Dan M. Roden[1,2,3], Joe-Elie Salem [1,4], Andrew M. Glazer†[1], Brett M. Kroncke†[1]

Affiliations:

[1]Department of Medicine, [2]Pharmacology, and [3]Biomedical Informatics, Vanderbilt University Medical Center, Nashville, TN, USA

[4]Clinical Investigation Center Paris-Est, CIC-1901, INSERM, Department of Pharmacology, Pitié-Salpêtrière University Hospital, Sorbonne Universite, 47 Boulevard de l'Hopital, Paris, France

[#]These authors contributed equally.

†Corresponding authors.

Corresponding authors:

Brett Kroncke, Ph.D.
Vanderbilt University School of Medicine
Medical Research Building IV, Rm. 1225
2215B Garland Ave
Nashville, TN 37232-0575
Email: brett.m.kroncke.1@vumc.org

Andrew Glazer. Ph.D.
Vanderbilt University School of Medicine
Medical Research Building IV, Rm. 1215
2215B Garland Ave
Nashville, TN 37232-0575
Email: andrew.m.glazer@vumc.org

Funding: This research was funded by the National Institutes of Health: R01HL160863 (BMK), R00HG010904 (AMG), and R35GM150465 (AMG); and by the Leducq Transatlantic Network of Excellence Program 18CVD05 (BMK)

Conflict of Interest: The authors declared no competing interests for this work

Keywords: Cardiology, Data Analysis, Dose response, ECG, In Vitro, Ion channels, Model evaluation, Pharmacology, Stem Cells, Translational Medicine

42 **ABSTRACT**

43 **Rationale:** Induced pluripotent stem cell-derived cardiomyocytes (iPSC-CMs) are an
44 emerging model for determining drug effects and modeling disease. Specialized devices
45 can generate Extracellular Field Potential (EFP) measurements from these cells,
46 analogous to the ventricular complex of the electrocardiogram.

47 **Objective:** The objective of this study was to develop an easy-to-use, easy-to-teach,
48 reproducible software tool to measure EFPs.

49 **Methods-Results:** We present the EFP-Analyzer (EFPA), a semi-automized analyzer for
50 EFP traces, which identifies and averages beats, identifies landmarks, and calculates
51 intervals. We evaluated the tool in an analysis of 358 EFP traces from 22 patient-derived
52 lines. We analyzed spontaneously beating iPSC-CMs, as well as optically paced iPSC-
53 CMs through channelrhodopsin. We developed stringent quality criteria and measured
54 EFP intervals, including Field Potential Duration (FPD). FPD from optically paced iPSC-
55 CMs were shorter than those of spontaneously beating iPSC-CMs (283.7.0±54.2 vs.
56 293.0±47.5, p: 0.32, respectively). We further analyzed the usability and data
57 replicability of EFPA through an inter-intra observer analysis. Correlation coefficient for
58 inter-reader tangent and threshold measurements for these FPD ranged between r: 0.93-
59 1.00. Bland-Altman plots comparing inter observer results for spontaneously beating and
60 paced iPSC-CMs showed 95% limits of agreement (−13.6 to 19.4ms and −13.2 to
61 15.3ms, respectively). The EFP-analyzer could accurately detect FPD prolongation due to
62 drug (moxifloxacin) or pathogenic loss of function mutations (*CACNA1C* N639T). This
63 program is available for download at https://github.com/kroncke-lab/EFPA. The

instructions will be available at the same listed website under the README section of the Github main page.

Conclusions: The EFP-Analyzer tool is a useful tool that enables the efficient use of iPSC-CMs as a model to study drug effects and disease.

68 **INTRODUCTION**

69 Since their discovery in 2006,[1] induced pluripotent stem cells (iPSCs) have
70 become a transformative tool for modeling cell behavior, drug response, and disease.[2] A
71 number of groups have developed methods for differentiating iPSCs into cardiomyocytes
72 (CMs).[3] These induced pluripotent stem cell derived cardiomyocytes (iPSC-CMs) are an
73 emerging model for the study of drug safety screening, in particular for detecting drugs
74 that prolong the cardiac action potential duration.[4,5] iPSC-CMs have also been used to
75 study genetic background variability in electrocardiographic properties and drug
76 response.[6] In addition, gene-editing methods such as clustered regularly interspaced short
77 palindromic repeats (CRISPR) allow further studies of mutation effects on iPSC-CMs.[7]
78 Advancements in optogenetic methods have allowed for the expression of
79 channelrhodopsin, a light activated ion channel, in iPSC-CMs to enable optical pacing.[8]
80 More accurate investigations of cardiac function and pharmacological effects make it
81 possible to precisely and non-invasively control cardiomyocyte activity. Although iPSC-
82 CMs are thought to represent a relatively immature state of cardiac differentiation, recent
83 methods have resulted in improved ventricular cardiomyocyte differentiation,
84 successfully profiling all major cardiac currents in iPSC-CMs.[9] The Extracellular Field
85 Potential (EFP) measures the ion movement across cell membrane during contraction via
86 adjacent electrodes.[10] EFP signatures directly represent a cardiomyocyte's beating pattern
87 and could be considered analogous to the electrocardiogram (ECG). Previous literature
88 defined the analogous time-based parameters as depolarization time (DT), repolarization
89 time (RT), and maximum field potential duration (FPDmax).[11]

90 ECG analysis software automation is widespread with extensive validation
91 regarding consistency of these measurements.[12] The heart has large conduction distances
92 and regions with distinct beating patterns, such as the atria, ventricles, and his-Purkinje
93 complexes. In contrast, iPSC-CM monolayers are a relatively uniform substrate with
94 small conduction distances. Although the EFP representation appears analogous to the
95 ventricular complex (Depolarization and Repolarization) of the ECG (Figure 1),
96 relatively little work has demonstrated the consistency or reliability of EFP
97 measurements, including intra and inter observer reliability. In addition, no standardized
98 analysis tools have been made to analyze EFP morphology and parameters. Previous
99 studies have adapted ECG analyzers such as LabChart designed for *in vivo* animal
100 analysis, used software built-in to the devices, or used custom analysis methods without
101 assessing reliability of these strategies.[13–15]
102 We present the EFP-Analyzer (EFPA), a semi-automated software tool for
103 analysis of EFP traces. We use the EFP-Analyzer to analyze a large dataset of 358 control
104 EFPs from 22 control patients and provide guidelines for stringent quality criteria. We
105 show that this tool is fast to use, and generates consistent, reliable measurements. The
106 EFP Analyzer can accurately detect changes in FPDmax from QT prolonging drug
107 (moxifloxacin) or mutation (CACNA1C N639T). This tool will help facilitate the use of
108 EFPs in iPSC-CMs for drug screening and disease modeling.

109 **Materials and Methods**

110 Generation of iPSC lines: Eight female and seven male patients with no known
111 congenital arrhythmia syndromes were chosen (Figure S1). All patient-derived lines
112 were generated with patient consent under Vanderbilt IRB #040551. Peripheral blood
113 mononuclear cells were isolated from blood and reprogrammed into iPSCs using
114 electroporation delivery (Neon system, ThermoFisher) of non-integrating episomal
115 vectors (Epi5 Episomal iPSC Reprogramming Kit, ThermoFisher). iPSC-like colonies
116 were manually moved to hES-grade matrigel (Corning) coated 24-well plates between
117 day 14-30 post-electroporation. Individual colonies were expanded for validation and line
118 maintenance. Selected iPSCs were validated by staining with OCT4 (Cell Signaling,
119 #2750), SSEA4 (DSHB, MC-813-70), SSEA3 (Millipore, MAB4303), and Tra1-60
120 (Millipore, MAB4360). All iPSC lines used in this study were karyotype normal
121 (Genetics Associates, Nashville, TN).
122
123 Cardiomyocyte differentiation: IPSC's were cultured in mTeSR media for 4-5 days to
124 achieve ~80% confluency. Media was changed to cardiac differentiation medium: RPMI
125 1640 (11875, Life Technologies), 2% B-27 minus insulin supplement (A1895601, Life
126 Technologies), and 1% Penicillin-Streptomycin (Life Technologies). From days 0-2 the
127 media was supplemented with 6 μM CHIR99021 (LC Laboratories), and from days 3-5
128 with 5 μM IWR-1 (Sigma). From days 13-19 metabolic selection medium was used:
129 RPMI1640 without glucose (11879, Life Technologies), 2% B-27 minus insulin
130 supplement (A1895601, Life Technologies), and 1% Penicillin-Streptomycin (Life
131 Technologies). For days 19+ cardiomyocyte media was used. Media was exchanged

132 every other day. Selected iPSC-CM were validated by staining with alpha-actinin
133 (Sigma). Optically paced cells were treated from days 28-30 with 6500 genome
134 copies/cell of AAV1.CAG.hChR2(H134R)-mCherry.WPRE.SV40 (Addgene20938M)
135 purchased from the University of Pennsylvania Vector Core. At day 30 cells were
136 replated into CardioExcyte96 sensor plates (Nanion) coated with 50 µl of 1:100 Matrigel,
137 and cells were studied at day 38-42 post-differentiation.
138
139 EFP measurement: EFP and impedance signals were measured on the CardioExcyte96
140 (Nanion) 8-12 days after replating (day 38-42 post-differentiation). Cells were kept at
141 37°C, 80% humidity, and 5% CO_2. For optical pacing, a stimulating optical lid (Nanion)
142 was used, which exposed all wells to 470nm wavelength light. Cells were exposed at 1
143 Hz to 5 msec-long pulses of light at 30 mA power. 20-30 second sweeps were recorded at
144 an acquisition rate of 0.1 ms. Raw EFP and impedance measurements were converted
145 into tab-delimited files and processed in the EFP-Analyzer tool.
146
147 EFP-Analyzer analysis: A flowchart of the analysis logic is presented in Figure 1. The
148 user is first presented with a data input screen (Figure 1) which allows the import of a tab
149 delimited file containing time in seconds in column 1 and EFP measurements from
150 multiple samples (wells) in columns 2+. Alternatively, the user can also load a previously
151 analyzed project. Upon loading the input files and selecting initial settings, screen 2 is
152 presented, which contains the main analysis. The top plot displays the entire sweep, from
153 which beats can be selected automatically or manually for analysis. Beats are averaged
154 and displayed in plot 2. Beats deviating from the mean beat by more than the noise cutoff

155 are eliminated. Landmarks for the DT complex, the T peak, the T_{end} tangent point, and
156 the T_{end} threshold point are selected automatically or manually (Figure 1). The user can
157 navigate between samples and choose which samples to include or exclude.
158 Measurements and plots can be downloaded to the user's computer as a series of .csv and
159 .pdf files. Additional EFP Analyzer features are described in the supplemental methods.
160
161 Analysis of control EFPs: 22 control lines were selected across 15 AAV-treated and 10
162 non-AAV treated lines (Figure 2). All EFPs were classified by morphology into one of 3
163 categories: standard, low amplitude, and biphasic (Figure 3). Low amplitude traces were
164 defined as traces with a repolarization wave maximal amplitude (T peak) less than 15 uV.
165 Biphasic traces were defined as those having two distinct repolarization waves in
166 opposite directions, each later than 50 ms after the beginning of depolarization.
167 Recordings were conducted in 20-30 second intervals at an acquisition rate of 0.1 ms.
168 The mean beat was defined by the average of the beginning of the depolarization time to
169 the end of the T wave from selected beats. Irregular traces were excluded, as standard,
170 repeatable beats were preferred to avoid the complexity of median representative beat
171 analysis. Optically paced traces not at 1 beat per second were excluded. Each EFP was
172 then measured with the EFP Analyzer tool as described above.
173
174 Analysis of EFPs after exposure to an IKr-Blocker or to pathogenic genetic variant in
175 CACNA1C: Moxifloxacin, a hERG channel blocker,[16] was applied to patient generated
176 iPSC-CMs without known congenital arrhythmogenic genetic background in increasing
177 doses (10 uM, 30 uM, 100 uM, 300 uM) at 1-hour intervals. The iPSC lines heterozygous

178 for CACNA1C N639T were generated as previously described.[11,17] Statistical analyses

179 were performed in R (version 4.1.2).

RESULTS

Description of EFP-Analyzer software tool

We developed the EFP-Analyzer software tool, a Shiny-based interactive tool, available for download at https://github.com/kroncke-lab/EFPA . The tool comprises two separate pages: a data load screen and a data analysis screen (Figure 1). In the data load screen, users upload a dataset of EFP signal versus time, formatted in a comma separated values (.csv) file, and select analysis parameters. In the data analysis screen, beats are selected and averaged, landmarks are placed and intervals are calculated. The philosophy of the program is that it is "semi-automated" and landmarks resemble to the one used to evaluate ventricular depolarization (QRS) and repolarization processes (QT) in human ECG. Therefore, these parameters are named DT and FPD (Figure 1). The program performs these tasks automatically once a new well is loaded. Users can modify the beat location and landmark placement.

Analysis of 22 iPSC-CM lines

We applied the EFP-Analyzer to EFPs generated from the CardioExcyte96, a 96-well plate format EFP generator from Nanion. We evaluated iPSC-CM lines derived from individuals without apparent genetic arrhythmia disorders. From the recorded 25 patient lines, we screened a total of 1280 traces (30 seconds per trace; 8-150 traces per patient line). Some traces were analyzed with spontaneous beating, and some were treated with an AAV-ChR and optically paced. From an initial dataset of 708 spontaneous and 572 optically paced traces, wells that were not beating or irregularly beating were excluded leaving 303 spontaneous and 55 AAV traces from 22 patient lines (Figure 2). We

203 determined the consistency of the EFP-Analyzer to measure FPDmax on EFP traces as a
204 function of EFP morphology classified into 3 categories (standard, low amplitude,
205 biphasic) (Figure 3). A random selection of 260 paced and 430 unpaced traces (stratified
206 by EFP repolarization morphology) were repeated in measurement by an expert (AG),
207 and by a novice (YW) who had a training session of 10 minutes in how to analyze the
208 data and use the tool (~10 EFP test measurements) (Figure 4). The consistency and bias,
209 the mean difference between repeat measurements as a function of morphology traces are
210 displayed in Table 2 and Table 3. The EFP with a standard morphology had the highest
211 level of measurements reproducibility while EFP with low amplitude or biphasic
212 morphology were poorly reproducible and highly scattered (Table 1).
213 Therefore, we focused for the subsequent analyses only on the EFPs with standard
214 trace morphology, 303 (303/708, 43%) spontaneous and 55 (55/572, 9.6%) high-quality
215 AAV-ChR traces which compose the main dataset. All traces were measured by an expert
216 analyzer (AG). Two methods were used, a simple threshold method and a tangent
217 method, based on the different DT, reflective of measurement techniques used in human
218 ECGs (Table 1). FPD assessment by tangent method was shorter and carried a lower
219 dispersion than the FPD assessed by threshold method (283.7±54.2 vs. 442.9±109.2, p:
220 <0.001, respectively, Table 1). Among the FPD (tangent method) measured by two
221 readers, Bland-Altman plots results showed 95% limits of agreement ranging from –13.6
222 to 19.4 ms and from -13.2 to 15.3 ms for spontaneously beating and paced iPSC-CMs,
223 respectively (Figure 5 and Table 2). Among the FPD (tangent method) measured by the
224 intra reader, Bland-Altman plots results showed 95% limits of agreement ranging from -
225 22.6 to 21.5 ms and from -17.4 to 17.0 ms for spontaneously beating and paced iPSC-

226 CMs, respectively (Figure 5 and Table 2). Correlation coefficient for inter reader
227 measurements for these FPD (tangent method) ranged between r:0.93-1.00 (Table 3).
228 EFP-FDP (tangent method) were shorter in the group of paced EFP vs. spontaneous EFP
229 (283.7±54.2 vs. 293.0±47.5, respectively) partly due to shorter EFP-DT in the group of
230 paced EFP vs. spontaneous EFP (26.4±14.7 vs. 58.9±21.6, respectively). Data concerning
231 Bland-Altman plots and intraclass correlation coefficient for intra- and inter-reader for
232 EFP-FPDmax measured by threshold method are provided in Table 2. Data concerning
233 differences between spontaneous and paced EFP for FPD measured by threshold method
234 shared the same trend that with FPD measured by tangent method and are displayed in
235 Table 1. Amongst the spontaneously beating and paced cells, FPD was not significantly
236 correlated with RR (spearman rho= 0.183, $p = 0.135$; and rho = -0.165, $p = 0.147$;
237 respectively, Figure S2).
238
239 Application to drug response and disease
240 We analyzed the EFP-Analyzer tool's ability to identify changes to EFP
241 pattern/landmarks in response to drugs and in the case of individuals with disease. We
242 first analyzed the action potential-prolonging drug moxifloxacin. We successfully
243 detected an increase in FPDmax in response to increasing doses of moxifloxacin, with
244 119 ± 9.9 ms prolongation at 100 uM (Figure 6). Next, we re-analyzed a previously
245 published cell line carrying a pathogenic Long QT Type 8 *CACNA1C* variant N639T.
246 Consistent with the previous study, relative to isogenic controls (non-CRIPSR edited) the
247 mutation positive cell line had FPDmax prolongation in optically paced cells, ($n = 15$
248 cells/line, $p < 0.002$, two-tailed t test, Figure 6).

249 **DISCUSSION**

250 Summary

251 The EFP-Analyzer (EFPA) aims to streamline cardiac disease modeling. We
252 showed consistency in measurements in interpretation of beats and landmarks across 22
253 patient lines with 358 traces. We were able to reliably detect pharmacological
254 (moxifloxacin) and pathological alterations (CACNA1C N639T) from functional
255 signatures. We further established strong inter-reader correlation coefficients (r:0.93-
256 1.00) and good agreement in Bland-Altman. This technology not only allows for high-
257 quality data capture, but it also ensures replicability across multiple users and studies[10],
258 representing a significant advancement in integrating iPSC-CMs in drug screening
259 paradigm. EFPA's versatility and convenience of use are critical for promoting wider
260 adoption in academic and pharmaceutical research, notably in improving the efficiency,
261 accuracy, and accessibility of EFP measurements.

262

263 The EFP Analyzer is a fast, consistent tool for data analysis

264 The data derived from EFPA is robust and consistent between multiple observers.
265 Analysis of 9 replicate sweeps in a 96 well plate was 12 ± 3 minutes. The mean
266 difference between observers was 20-25 ms for unpaced and 8-12 ms for paced cells.
267 This approaches the robustness achievable in an ECG's QTc, typically considered to be
268 around 11.8 ms.[12] We speculate that uniform synchronous depolarization of an entire well
269 using optical pacing resulted in a more repeatable (and 25 ms shorter) FPDmax than
270 spontaneous cell activation in a well, which requires the signal to spread throughout the
271 well from a point of activation.

272

273 Recommendations for improving EFP quality/robustness

274 We observed a range of EFP morphologies, which we termed standard, low
275 amplitude, and biphasic. We found that according to a variety of metrics, low amplitude
276 and biphasic EFPs generated non-robust data, leading to highly variable, inconsistently
277 measured values. We therefore recommend that these classes be removed. The tangent
278 approach also improved the robustness of the EFPs according to these metrics. We note
279 that these parameters were optimized on EFPs generated from one device, the Nanion
280 CardioExcyte 96. Alternative cardiac screening instruments may differ in system defaults
281 such as sampling rates, leading to potential differences in results.

282 For ECG analysis, a return to baseline of the QT is commonly used with multiple
283 input convergence. However, in some cases the T wave has an extended unclear return to
284 baseline particularly the lower the T peak is in term of amplitude, and a tangent method
285 (drawn at the steepest point) yields more robust FPD measurements.[18] We observed that
286 some EFPs had long extended repolarization waves, analogous to T waves in the ECG.
287 Thus, we employ the tangent method and observed a decrease in the standard deviation of
288 the tangent and threshold method across many wells, which suggests both approaches are
289 accurate/repeatable; we similarly observed more robust measurements when comparing
290 across multiple observers.

291

292 Comparison to other methods/tools

293 The CardioExcyte 96 has well been defined by several groups in high throughput
294 genomic and pharmacological investigations and has since proven to be invaluable across

295 disciplines[3,17,19–21]. It has built-in software to calculate intervals, however we found that
296 the EFP Analyzer was a better fit for analyzing the data flexibly and storing and
297 managing the data. The EFP Analyzer has increased capabilities, such as the tangent
298 method, an option to manually adjust the beat locations, and persistent data storage.
299 Additionally, the EFP analyzer standardizes the baseline start for each complex and
300 allows for additional analyses such as calculating T-Amp, therefore increasing the
301 accuracy of evaluations. Another advantage of the EFP Analyzer is that it is semi-
302 automated; for many traces it correctly identifies all the landmarks without any manual
303 changes. Other EFPs with complicated/unclear patterns or with high background/artifact
304 need manual intervention to optimize. Another advantage is that it also functions as a
305 data organizer that saves data which simplifies analysis, reviewing, and editing steps for
306 collaborating researchers.
307
308 Limitations
309 The ability of this software to analyze EFP repolarization wave characteristics
310 was demonstrated in our investigation. Even though T peak amplitude and T peak T_{end}
311 are important clinical metrics, we did not test the capability to analyze these
312 characteristics.[12] Furthermore, we did not study HR dependence of field potential
313 duration. We observed a RT-peak amplitude decrease with moxifloxacin incubation,
314 which calls for further investigation. Additionally, this method has also been compatible
315 with *CACNA1C* N639T, a cell line with a congenital Long QT syndrome type 8. This
316 program was customized for Nanion CardioExcyte 96 device and datasets with
317 fundamentally similar EFP shapes. Data processing devices with differing EFP

characteristic output, such as MEAs, may pose as a limitation. Future research is needed to test this and discover the software's maximum capabilities. We encourage software limit testing to discover maximum capabilities. All comments, suggestions, and feedback for EFP-Analyzer can be submitted on https://github.com/kroncke-lab/EFPA/issues.

322 **REFERENCES**

323 1. Takahashi K, Yamanaka S. Induction of Pluripotent Stem Cells from Mouse
324 Embryonic and Adult Fibroblast Cultures by Defined Factors. *Cell*. 2006;126(4).
325 doi:10.1016/j.cell.2006.07.024

326 2. Shi Y, Inoue H, Wu JC, Yamanaka S. Induced pluripotent stem cell technology: A
327 decade of progress. *Nat Rev Drug Discov*. 2017;16(2). doi:10.1038/nrd.2016.245

328 3. Denning C, Borgdorff V, Crutchley J, et al. Cardiomyocytes from human
329 pluripotent stem cells: From laboratory curiosity to industrial biomedical
330 platform. *Biochim Biophys Acta Mol Cell Res*. 2016;1863(7).
331 doi:10.1016/j.bbamcr.2015.10.014

332 4. Vicente J, Zusterzeel R, Johannesen L, et al. Mechanistic Model-Informed
333 Proarrhythmic Risk Assessment of Drugs: Review of the "CiPA" Initiative and
334 Design of a Prospective Clinical Validation Study. *Clin Pharmacol Ther*.
335 2018;103(1). doi:10.1002/cpt.896

336 5. Millard D, Dang Q, Shi H, et al. Cross-site reliability of human induced pluripotent
337 stem cell-derived cardiomyocyte based safety assays using microelectrode arrays:
338 Results from a blinded cipa pilot study. *Toxicological Sciences*. 2018;164(2).
339 doi:10.1093/toxsci/kfy110

340 6. Stillitano F, Hansen J, Kong CW, et al. Modeling susceptibility to drug-induced
341 long QT with a panel of subject-specific induced pluripotent stem cells. *Elife*.
342 2017;6. doi:10.7554/eLife.19406

343 7. Garg P, Oikonomopoulos A, Chen H, et al. Genome Editing of Induced Pluripotent
344 Stem Cells to Decipher Cardiac Channelopathy Variant. *J Am Coll Cardiol*.
345 2018;72(1). doi:10.1016/j.jacc.2018.04.041
346 8. Dwenger M, Kowalski WJ, Ye F, et al. Chronic optical pacing conditioning of h-iPSC
347 engineered cardiac tissues. *J Tissue Eng*. 2019;10.
348 doi:10.1177/2041731419841748
349 9. Parikh SS, Blackwell DJ, Gomez-Hurtado N, et al. Thyroid and Glucocorticoid
350 Hormones Promote Functional T-Tubule Development in Human-Induced
351 Pluripotent Stem Cell-Derived Cardiomyocytes. *Circ Res*. 2017;121(12).
352 doi:10.1161/CIRCRESAHA.117.311920
353 10. Halbach MD, Egert U, Hescheler J, Banach K. Estimation of action potential
354 changes from field potential recordings in multicellular mouse cardiac myocyte
355 cultures. *Cellular Physiology and Biochemistry*. 2003;13(5).
356 doi:10.1159/000074542
357 11. Chavali N V., Kryshtal DO, Parikh SS, et al. Patient-independent human induced
358 pluripotent stem cell model: A new tool for rapid determination of genetic variant
359 pathogenicity in long QT syndrome. *Heart Rhythm*. 2019;16(11).
360 doi:10.1016/j.hrthm.2019.04.031
361 12. Saqué V, Vaglio M, Funck-Brentano C, et al. Fast, accurate and easy-to-teach QT
362 interval assessment: The triplicate concatenation method. *Arch Cardiovasc Dis*.
363 2017;110(8-9). doi:10.1016/j.acvd.2016.12.011

364 13. Patejdl R, Gromann A, Bänsch D, Noack T. Effects of ajmaline on contraction
365 patterns of isolated rat gastric antrum and portal vein smooth muscle strips and
366 on neurogenic relaxations of gastric fundus. *Pflugers Arch*. 2019;471(7).
367 doi:10.1007/s00424-019-02279-y
368 14. Printemps R, Guilbot S, Didier H, Nalin R, Le Grand B. The Cardiotoxic Effect of
369 Roundup® is not Induced by Glyphosate: A Non-specific Blockade of Human
370 CaV1.2 Channels. *Cardiovasc Toxicol*. 2022;22(7). doi:10.1007/s12012-022-09749-
371 3
372 15. Wei X, Chang ACH, Chang H, et al. Hypoglycemia-Exacerbated Mitochondrial
373 Connexin 43 Accumulation Aggravates Cardiac Dysfunction in Diabetic
374 Cardiomyopathy. *Front Cardiovasc Med*. 2022;9. doi:10.3389/fcvm.2022.800185
375 16. Alexandrou AJ, Duncan RS, Sullivan A, et al. Mechanism of hERG K + channel
376 blockade by the fluoroquinolone antibiotic moxifloxacin. *Br J Pharmacol*.
377 2006;147(8). doi:10.1038/sj.bjp.0706678
378 17. Clements M, Thomas N. High-throughput multi-parameter profiling of
379 electrophysiological drug effects in human embryonic stem cell derived
380 cardiomyocytes using multi-electrode arrays. *Toxicol Sci*. 2014;140(2).
381 doi:10.1093/toxsci/kfu084
382 18. Lester RM, Paglialunga S, Johnson IA. QT assessment in early drug development:
383 The long and the short of it. *Int J Mol Sci*. 2019;20(6). doi:10.3390/ijms20061324

384 19. Wang Y, Yao F, Wang L, et al. Single-cell analysis of murine fibroblasts identifies
385 neonatal to adult switching that regulates cardiomyocyte maturation. *Nat*
386 *Commun*. 2020;11(1). doi:10.1038/s41467-020-16204-w
387 20. del Álamo JC, Lemons D, Serrano R, et al. High throughput physiological screening
388 of iPSC-derived cardiomyocytes for drug development. *Biochim Biophys Acta Mol*
389 *Cell Res*. 2016;1863(7). doi:10.1016/j.bbamcr.2016.03.003
390 21. Wang H, Wang Y, Li J, et al. Three tyrosine kinase inhibitors cause cardiotoxicity
391 by inducing endoplasmic reticulum stress and inflammation in cardiomyocytes.
392 *BMC Med*. 2023;21(1). doi:10.1186/s12916-023-02838-2
393
394

Figure 1. EFP Analyzer Software User Interfa

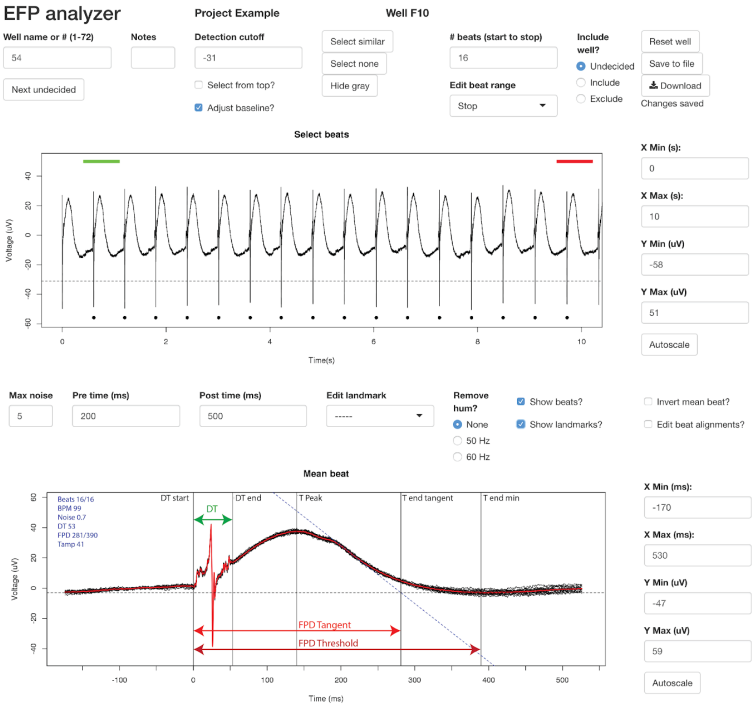

Figure 2. Flow Analysis Chart of Morphology between AAV-Chr & no AAV-Chr

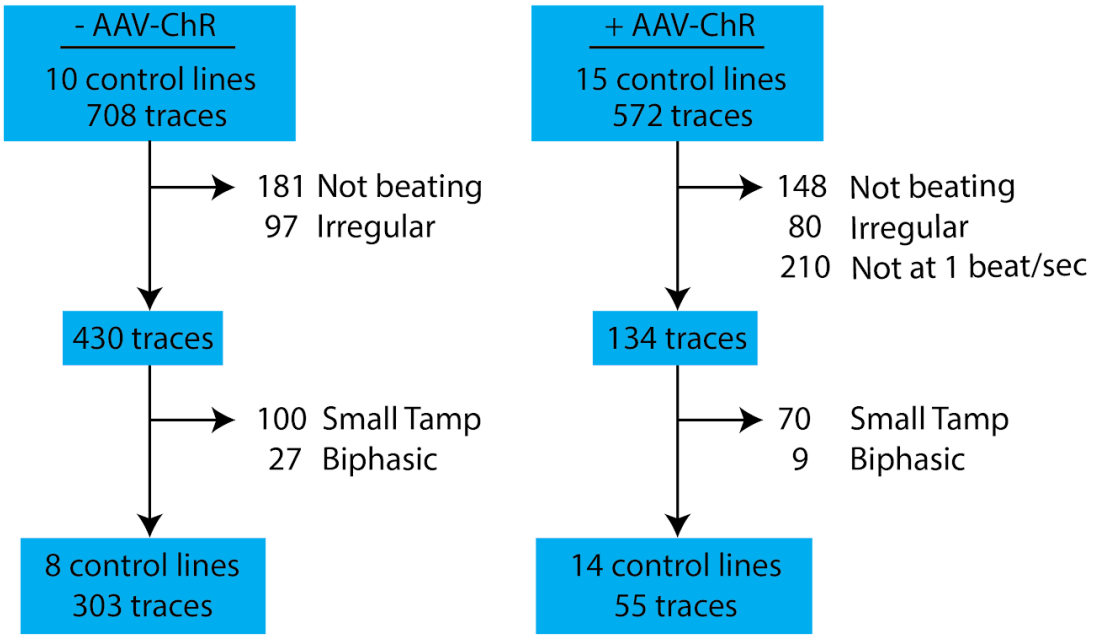

399 Figure 3. EFP Morphologies for Spontanously Beating and Paced Cells

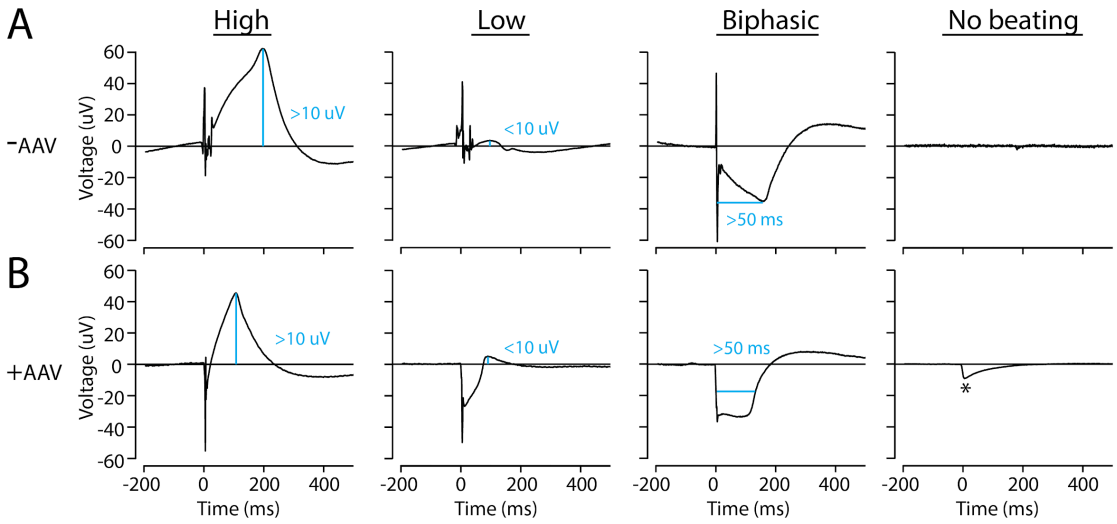

400

401 A) Example EFP morphologies for spontaneously beating cells (-AAV)

402 B) Example EFP morphologies for paced cells (+AAV). * Indicates a light pacing

403 artifact.

404

Figure 4. Flow Analysis Chart of Inter and Intra-Reader Variability Assessment

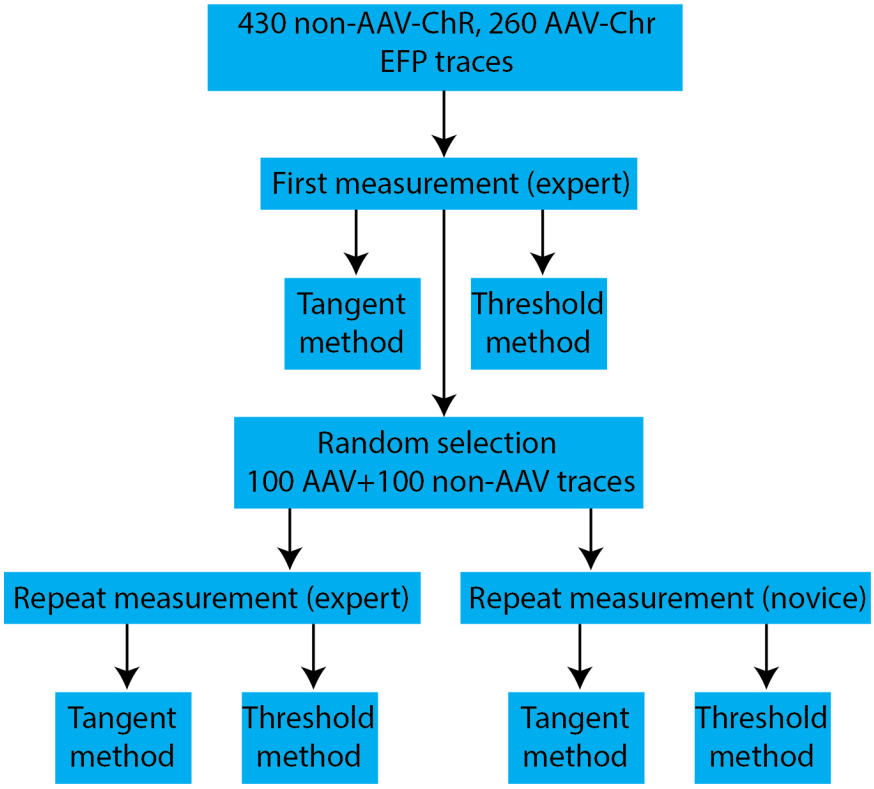

Figure 5. Comparison in FPD (ms) between Intra and Inter Reader

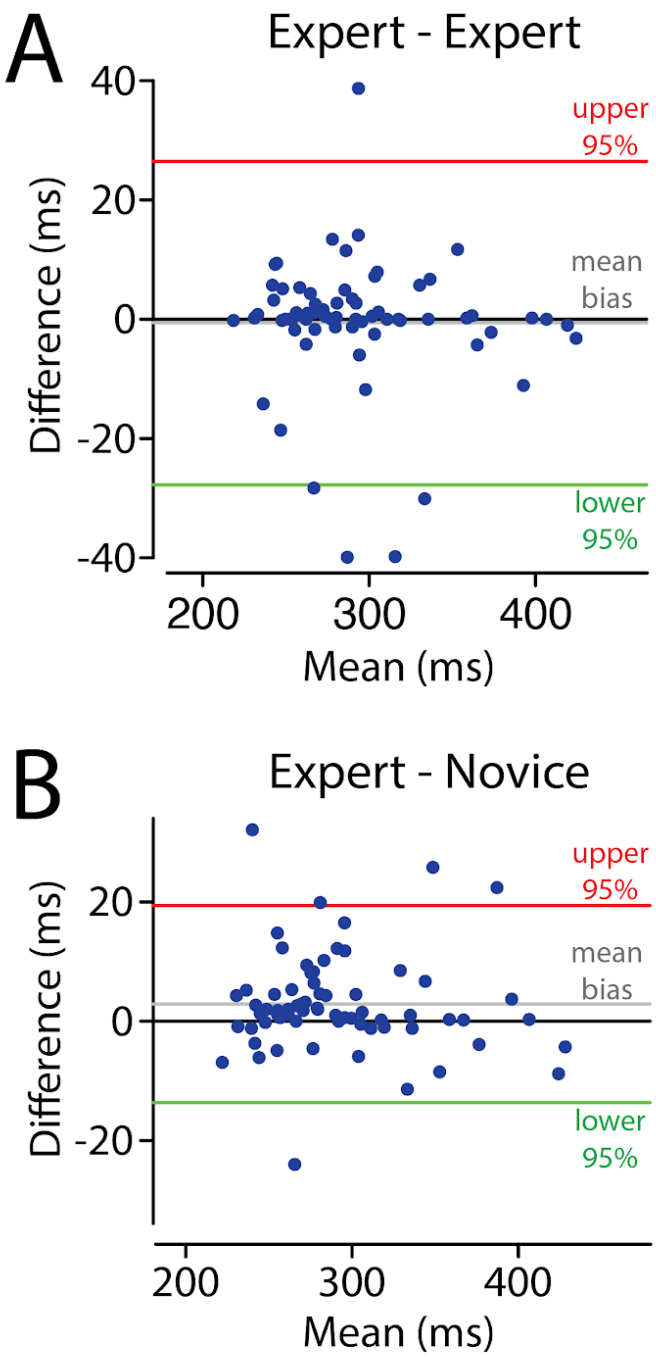

A) Difference in FPD (ms) between intra-reader (expert-expert)

B) Difference in FPD (ms) between inter-reader (expert-novice)

411 Figure 6. FPD response in an exposure to IKr Blocker and CACNA1C N639T

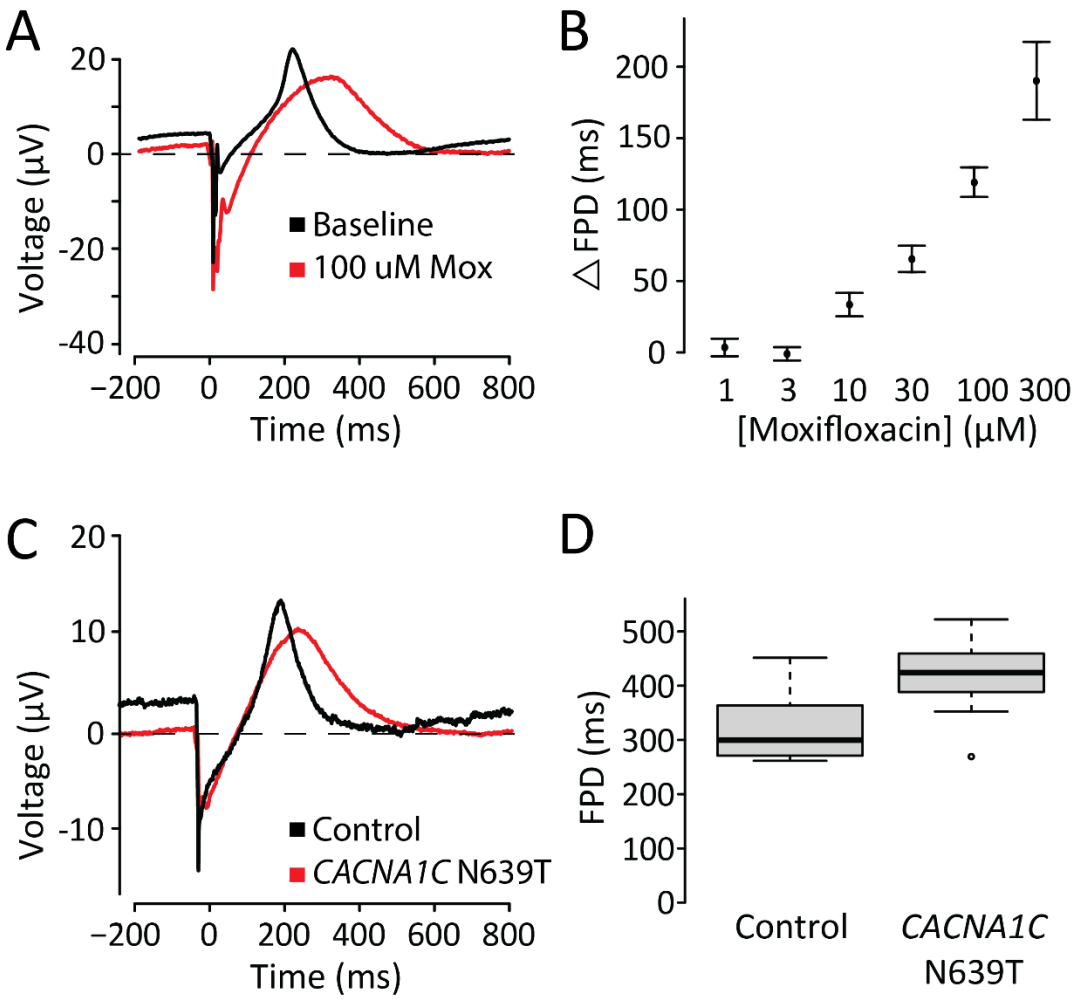

412

413 A) Representative EFP trace from an example cell treated with 100uM Moxifloxacin.

414 B) As the doses of Moxifloxacin increased, the change in QT was measured. Each

415 measurement represents n= 11 cells.

416 C) Representative EFP trace from an example N639T mutation positive cell.

417 D) The mutation positive cell line had prolongation in optically paced cells, (n = 15) cells

418 expressing CACNA1C N639T mutation exhibit a prolonged FPD compared to control

419 cells (n = 19).

420 **Table 1.**

421 Comparison of EFP parameters based on morphology & measurement method

422

AAV-ChR	Morphology	Number of wells	RR (ms)	EFP-DT	FPD tangent	FPD threshold	FPD tangent vs. threshold p-values
No	Standard	303	798.6(314.3)	58.9 (21.6)	293.0 (47.5)	461.0 (82.1)	<0.001
	Small Tamp	100	778.0(202.2)	59.8 (17.9)	466.3 (170.6)	603.5 (174.2)	0.06
	Biphasic	27	839.1(512.4)	108.5 (123.5)	602.9 (280.4)	736.1(349.3)	0.96
Yes	Standard	55	995.4(4.99)	26.4 (14.7)	283.7 (54.2)	442.9(109.2)	<0.001
	Small Tamp	21	993.7(4.93)	29.8 (28.1)	542.8(182.2)	690.2 (185.9)	0.01
	Biphasic	2	994.7(6.65)	45.2 (26.7)	369.9 (120.3)	690.3 (199.1)	0.22
AAV-ChR (Yes vs. No) p-values	Standard	NA	<0.001	<0.001	0.32	0.31	NA
	Small Tamp		<0.001	<0.001	0.16	0.02	
	Biphasic		0.42	0.91	0.14	0.69	

423 The numbers represent mean (standard deviation). *Abbreviations*: AAV: adeno-associated virus; EFP: extracellular field potential,

424 iPSC-CM: induced pluripotent stem-cell derived cardiomyocyte, CRISPR: clustered regularly interspaced short palindromic repeats;

425 FPD: Field Potential Duration; RR: time between two successive waves from the start of DT.

Table 2.

Comparison of EFP consistency based on inter and intra reader and measurement method

AAV-ChR	Morphology	Number of wells analyzed	FPD tangent consistency intra-reader (ms)	FPD tangent consistency inter-reader (ms)	FPD threshold consistency intra-reader (ms)	FPD threshold consistency inter-reader (ms)
No	Standard	68	-0.6 (11.2)	2.3(13.1)	-3.6(21.3)	3.9(23.4)
	Small Tamp	24	-2.0 (15.9)	-2.8 (47.1)	-9.1(25.5)	19.5(28.8)
	Biphasic	8	-18.7 (64.9)	-39.2 (104.5)	-32.9(39.6)	30.6(126.1)
Yes	Standard	73	-0.7 (8.6)	1.0 (7.3)	-0.1(5.6)	-0.2(10.8)
	Small Tamp	25	-5.2 (36.0)	-6.5 (43.3)	0.7(5.5)	-7.3(34.3)
	Biphasic	2	-2.4 (27.4)	8.5 (12.0)	-31.2(44.1)	-31.2(44.1)

Abbreviations: ChR: channelrhodopsin

Table 3.

Comparison of FPD consistency based on inter and intra reader and measurement method

AAV-ChR	Morphology	Number of wells analyzed	Intra Correlation Coefficients FPD tangent consistency	Inter Correlation Coefficients FPD tangent consistency	Intra Correlation Coefficients FPD threshold consistency	Inter Correlation Coefficients FPD threshold consistency
No	Standard	68	0.97	0.96	0.97	0.95
	Small Tamp	24	1.00	0.98	0.99	0.98
	Biphasic	8	0.97	0.93	0.99	0.96
Yes	Standard	73	0.99	0.99	1.00	1.00
	Small Tamp	25	0.98	0.98	1.00	0.99
	Biphasic	2	1.00	1.00	1.00	1.00

Abbreviations: Intra: collected values from one reader; Inter: differences between collected values from different readers

457 **Supplementary Figure 1**

458 Patient Demographic Information

459

A

Sex	Race	Ethnicity	Age at Time of Enrollment
Female	White	Non-Hispanic	39
Female	White	Non-Hispanic	52
Female	White	Non-Hispanic	62
Female	White	Non-Hispanic	67
Female	White	Non-Hispanic	69
Female	White	Non-Hispanic	69
Female	White	Non-Hispanic	75
Female	White	Non-Hispanic	76
Male	White	Non-Hispanic	23
Male	White	Non-Hispanic	26
Male	White	Non-Hispanic	39
Male	Black	Non-Hispanic	59
Male	White	Non-Hispanic	59
Male	White	Non-Hispanic	67
Male	White	Non-Hispanic	72

B

	n	Mean (Years of Age)	Standard Deviation
Total	15	56.93	17.36
Female	8	63.63	12.51
Male	7	49.29	19.82

C

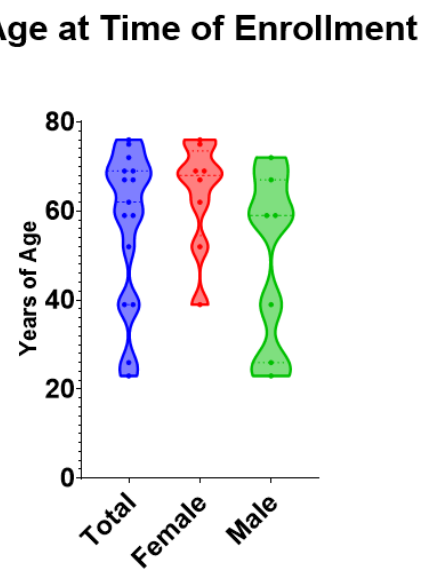

460

461 A) Enrolled patient demographic: sex, race, ethnicity, and age of enrollment

462 B) Mean patient age showing total n=15, female n=8, and male n=7

463 C) Volin plot depicting patient age at time of enrollment

Supplementary Figure 2

Comparison of RR and Field Potential Duration for Paced and Unpaced Cells

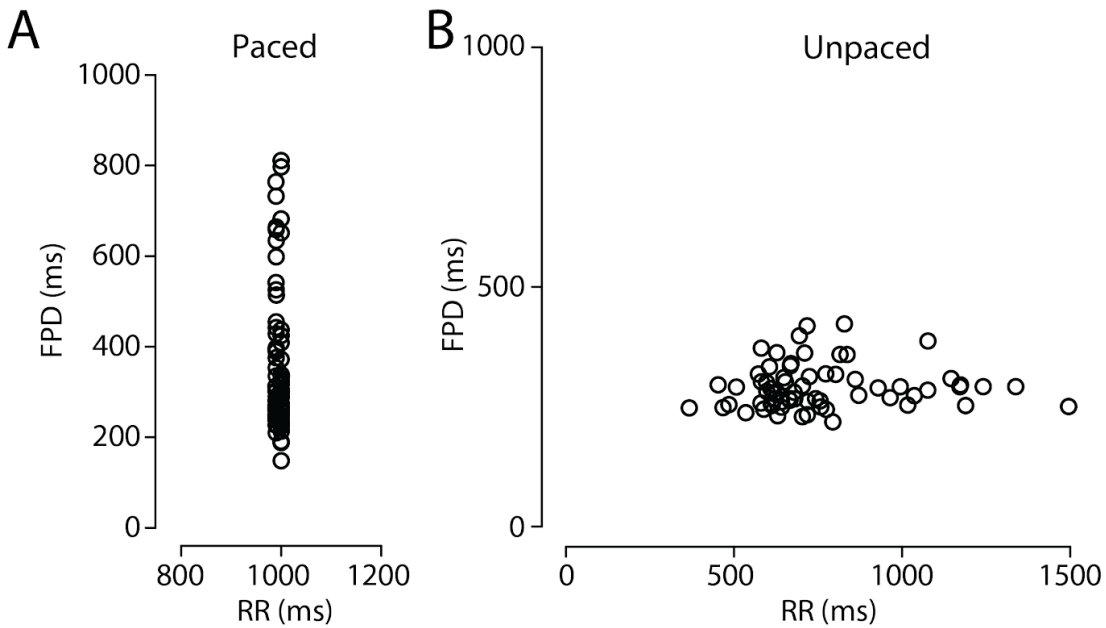

A) Paced cells spearman's rank correlation rho : S = 92171, p-value = 0.1474, rho = -0.165

B) Unpaced cells spearman's rank correlation rho : S = 42805, p-value = 0.1352, rho= 0.183